24th INTERNATIONAL CONGRESS ON SOUND AND VIBRATION
23–27 July 2017, London

RESEARCH ON RAIL CORRUGATION BASED ON STANDING WAVE THEORY

Xu Ning

luoyang sunrui rubber&plastic science and technology CO.LTD ,Luoyang, Henan, CHINA
email: xuning4243@163com

Wang Anbin

luoyang sunrui rubber&plastic science and technology CO.LTD ,Luoyang, Henan, CHINA

email: wangab725@163.com

This paper using the major domestic subway corrugation test data results, sums up the wave characteristics of rail corrugation conditions and simulation test systems, based on the laboratory test track, the vibration characteristics of the track system under different loading conditions, characteristics of fluctuation analysis, track system loads and puts forward the theory of how the rail corrugation wave occurs and the mechanism of the final product development that can be used to suppress the rail vibration and rail corrugation.
Keywords: rail corrugation, standing wave

1. Introduction

Rail corrugation is regular uneven wear waveform along the rail longitudinal on the top tracks, as shown in Figure 1. Rail corrugation not only causes strong vibration and noise, but also increases the cost of maintenance. Therefore, many scholars pay more and more attention to the cause of rail corrugation, and form a lot of valuable wave formation hypothesis and analysis model.

The corrugation characteristics are: rail corrugation usually occurs in damping fastening; They occurs in the radius of less than 400m of the circular curve on the rail top, and from the curve to the circular curve is gradually increasing; They occurs in the uniform speed section, braking and deceleration sections without corrugation; When the vehicle speed is adjusted, the rail corrugation is transferred from the current fastener to another type fastener zone[1].

Xu Ning[2], Wang Anbin proposed by fractal theory to study the rail corrugation, according to a number of domestic city subway line corrugation test data. As shown in Figure 2, the solution is the fractal of normal rail and rail corrugation of the extracted characteristic parameters, calculate the relationship between wheel and rail vibration field distribution under the similarities and differences, so as to study the mechanism of rail corrugation.

Figure 1: rail corrugation.

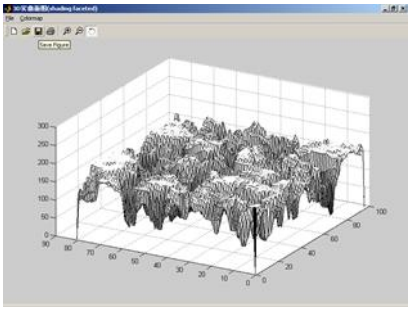

Figure 2: space model.

Due to limited precision by optical scanning equipment, we used the CAT apparatus to test rail corrugation. According to the characteristics of rail surface wear, we proposed a new method based on the theory of standing wave.

In this paper, according to the n order frequency of the wheel rail coupling vibration, we deduced the mechanism of rail corrugation, combined with the excitation frequency and the natural frequency of the rail system. In the laboratory, the tests were carried out by the rail hammering and deformation test, which used to confirm the theory.

2. Basic theory

2.1 Standing wave

Two rows of the same frequency, the same wavelength but in the opposite direction of the wave superposition, the displacement was:

$$u(x,t) = A_{+}e^{i(kx-\omega t+\gamma_{+})} + A_{-}e^{i(kx+\omega t+\gamma_{-})}. \tag{1}$$

Among them, A_+ and A_- are real amplitude; γ_+ andγ_- are phase angle. If $A_+=A_-=A$, then

$$\begin{aligned} u(x,t) &= Ae^{i(kx+0.5*\gamma_{+}+0.5*\gamma_{-})}\left[e^{-i(\omega t-0.5*\gamma_{+}+0.5*\gamma_{-})} + e^{i(\omega t-0.5*\gamma_{+}+0.5*\gamma_{-})}\right] \\ &= 2A\exp\left[i\left(kx+0.5*\gamma_{+}+0.5*\gamma_{-}\right)\right]\cos\left(\omega t-0.5*\gamma_{+}+0.5*\gamma_{-}\right) \end{aligned}. \tag{2}$$

The real part was:

$$u(x,t) = 2A\cos\left(kx+0.5*\gamma_{+}+0.5*\gamma_{-}\right)\cos\left(\omega t-0.5*\gamma_{+}+0.5\gamma_{-}\right). \tag{3}$$

At the point of $cos(kx+0.5*\gamma_{+}+0.5*\gamma_{-})=0$, the two traveling waves always cancel each other, while the medium is stationary.

2.2 Several formulas for frequency

1) the relationship of the corrugation excitation frequency, wavelength and speed are:

$$f_v = v/\lambda. \tag{4}$$

In the formula: f_v is the corrugation excitation frequency, v is speed, λ is wave length.

2) the natural frequency of the track system are:

$$f_s = \sqrt{k/m}. \tag{5}$$

In the formula: f_s is track system natural frequency, k is system stiffness, m is system quality.

2.3 Curve superelevation

For a curve with a certain radius, the superelevation have the following relations with the train speed:

$$h = 11.8v^2/R. \tag{6}$$

In the formula, v is the speed, R is the curve radius.

2.4 Beam vibration equation

The longitudinal vibration equation of the beam is:

$$\frac{\partial^2\xi}{\partial x^2} = \frac{1}{c_v^2}\frac{\partial^2\xi}{\partial t^2}. \tag{7}$$

In the formula, ξ is longitudinal deformation; c_v is speed of longitudinal waves.

The lateral vibration equation of the beam is:

$$\frac{\partial^4 \eta}{\partial x^4} + \frac{1}{c_s^2 K^2} \frac{\partial^2 \eta}{\partial t^2} = 0. \tag{8}$$

In the formula, K is the radius of gyration; η are each point on the beam from equilibrium distance; c_s is lateral wave propagation velocity.

3. Experimental test

3.1 Hammering test

As shown in Figure 3, through the hammer test, we can analyse the vibration energy transfer law and the transfer response function. The hammer test excitation positions were above fastener and intermediate of the two fasteners respectively. The testing conditions were mainly divided into load and no load, and the load for the simulation of A and B type train two effect of axial load effect on track system.

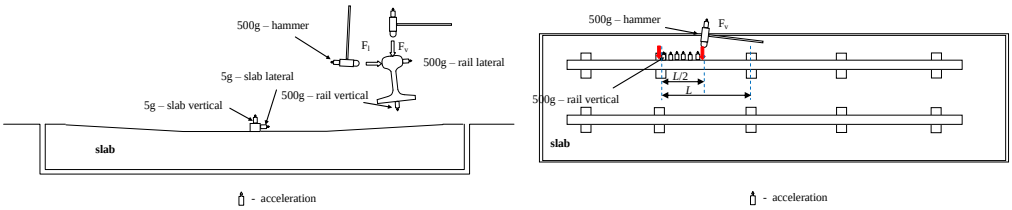

a) transfer response test b) energy transfer test

Figure 3: rail hammer test.

3.2 Corrugation test

The rail corrugation is the characteristic of the rail surface wear, which can be regarded as the macroscopic manifestation of the rail vibration characteristics. In this paper, the rail corrugations were tested at the distance of 25mm, 30mm, 35mm and 40mm from the rail, which used to analyse the fluctuation of the space rail corrugation.

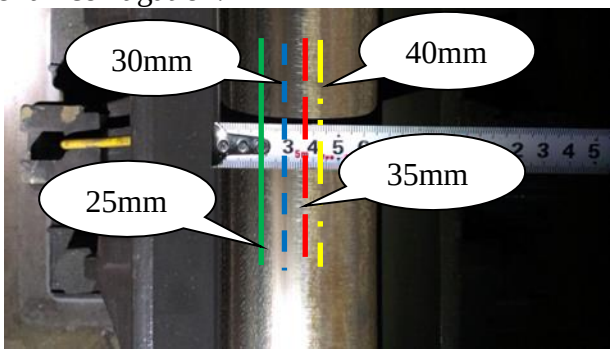

Figure 4: corrugation test.

3.3 Deformation test

The relative deformations of rail-ballast were measured by the displacement sensor, each sensor probe perpendicular to the measuring surface, measured as shown in figure 5.

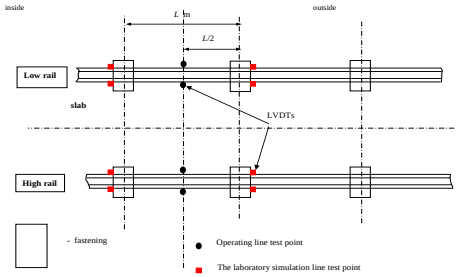

Figure 5: rail deformation test.

3.4 Laboratory 1:1 simulation track system

The system is shown in figure 6. The tests were carried out in two kinds of working conditions, namely, the load and no-load conditions. The test items mainly include hammer test and rail deformation test.

Figure 6: laboratory 1:1 simulation track system.

4. Test results

4.1 Hammering test results

4.1.1 Vibrational energy transfer

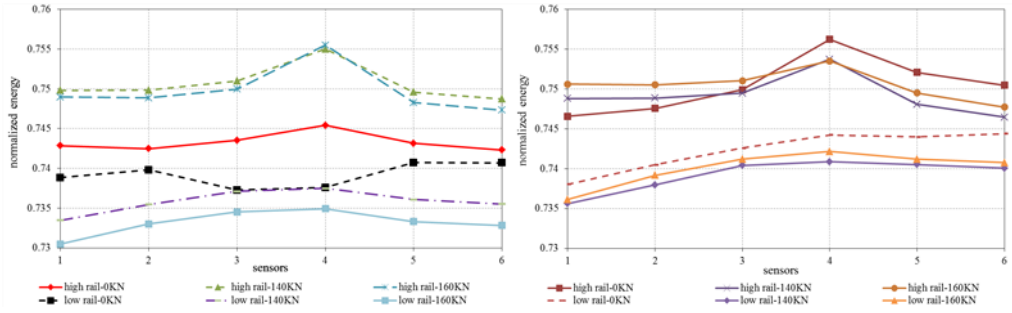

a) excitation above fastener b) intermediate of the two fasteners

Figure 7: mid-high frequency vibrational energy transfer.

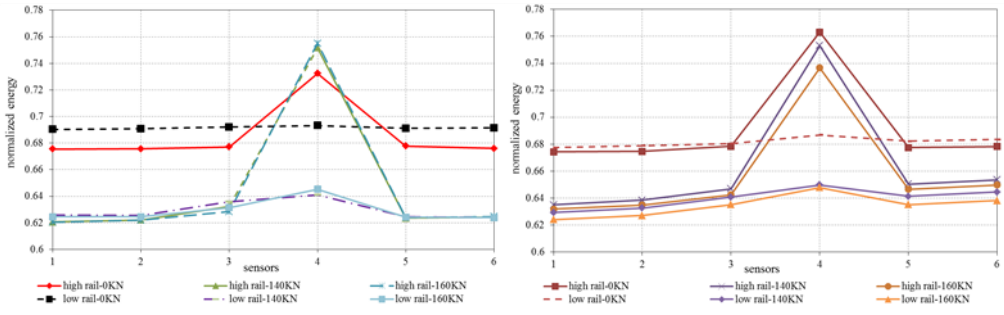

a) excitation above fastener b) intermediate of the two fasteners

Figure 8: low frequency vibrational energy transfer.

The sensors layout shown in Figure 3b), the numbers of sensor from left to right respectively were 1-6 sensors. The vibration energy transfer law of the rail can be obtained after the test of the total vibration level is normalized, as shown in the Figures 8, 9.

It can be seen from the figure that the fastener can transmit the rail vibration energy, so the energy ratio is less than 1 of the each sensor collect signal and the excitation signal. The normalized energy of the 6 signals presents half wave on the whole, and the signal of fourth sensor is the biggest. It is shown that the vibration propagates forward in a sine wave mode in the discontinuous support with the same interval.

Under different load conditions, the vibration energy of the high rail is higher than that of the low rail, which indicates that the energy damping of the rail is lower. In the Figure 8, the larger the load, the smaller the vibration energy. However, in the Figure 7, the situation is more complex in the middle and high frequency.

As a whole, it is shown that the vibration is transmitted by a standing wave mode at a single point excitation system, and the load affects the energy transfer.

4.1.2 Rail transfer response

Figure 9-11 are the rail transit response curves of the 0KN, 140KN and 160KN loading conditions. It can be seen that, under 0KN load, the response curves of the high and low rail are basically the same, the natural frequency was 152.4Hz of the high rail, and 146.5Hz of the low rail. The P-P frequency is near the 1007Hz both of high and low rail. When the load is applied, the response curves of the system are changed, it is no longer overlapped after the natural frequency, but they are basically the same as 140KN and 160KN. In addition, compared with the 0KN load, the natural frequency of the high rail is 164.1Hz, but there is no significant peak in the low rail. The P-P frequency of the low rail does not change, but the high rail is not obvious.

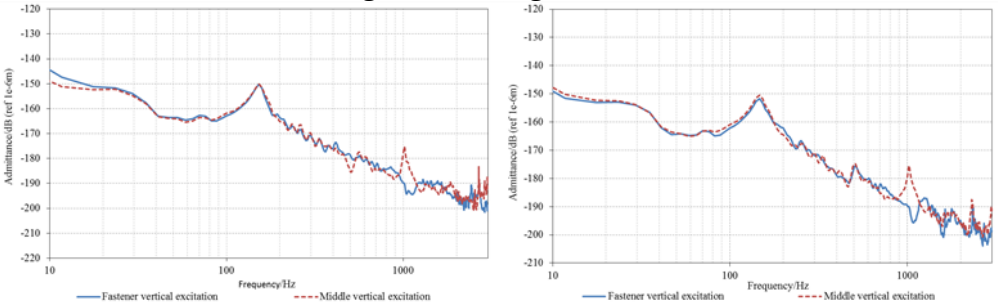

a) high rail b) low rail

Figure 9: Rail transfer response under 0KN load.

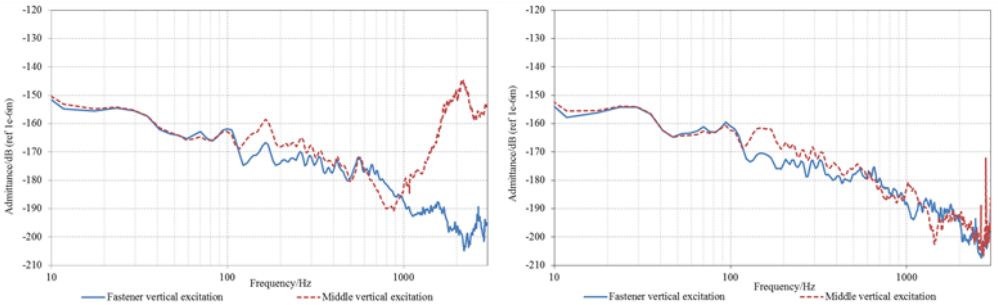

a) high rail b) low rail

Figure 10: Rail transfer response under 140KN load.

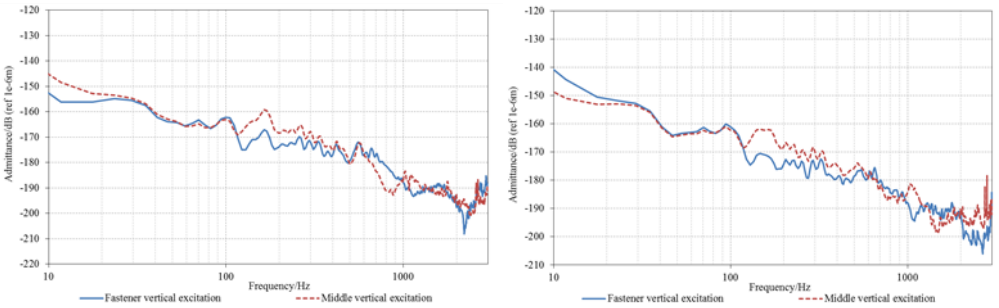

a) high rail b) low rail

Figure 11: Rail transfer response under 160KN load.

4.2 Corrugation test results

Figure 12 is the corrugation tracking test results, which in July 8th for a rail grinding. It can be seen the high rail corrugation roughness decreased of the distance from 25mm to 40mm, the low rail nearly the same. This means that the high rail distance is inclined to the inside of the rail, and the low rail is basically in the middle.

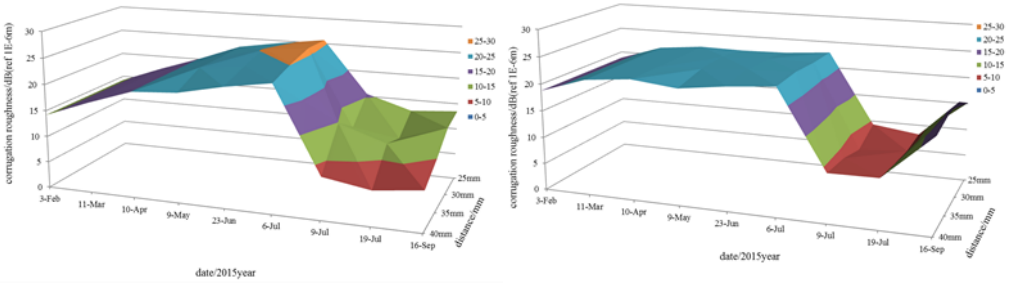

a) high rail b) low rail

Figure 12: Rail corrugation roughness.

4.3 Deformation test results

Table 1 is the rail deformation date of the under different load conditions in the laboratory. Table 2 is the rail deformation date of the operating line, that the vehicle axle load was 16T, corresponding to the laboratory 160KN load conditions.

Table 1: Rail deformation in the laboratory simulation system

	low rail		high rail		difference	
	outside	inside	outside	inside	outside	inside
0KN	-1.85	-1.94	-1.85	-1.81	0.00	0.13
140KN	-2.21	-2.28	-2.16	-2.14	0.04	0.14
160KN	-2.54	-2.59	-2.45	-2.44	0.09	0.15

Note: the difference was high rail deformation subtracts low rail, and negative means that the rail sinks.

Table 2: Rail deformation of the Metro Line

	low rail		high rail		difference	
	outside	inside	outside	inside	outside	inside
driving shaft	-2.44	-0.30	-2.32	-1.06	0.12	-0.78
driven shaft	-1.50	-1.25	-2.00	-1.40	-0.50	-0.15
average	-1.97	-0.78	-2.16	-1.23	-0.19	-0.45

Note: 1) the difference was high rail deformation subtract low rail, and negative means that the rail sinks.
2) the average was between the date of driving shaft and driven shaft.

In the table 1, the rail deformation increases with the load increase, and the deformation of the lower rail is higher than that of the high rail under the same load. The larger the deformation is, the

larger the stiffness is, that lead to the vibration damping, therefore coincide with the high rail energy is greater than low rail. The reasons are boosting point rail bias inside of the different deformation both sides of rail.

Table 2 the low rail deformation is less than the high rail deformation, coincide with the high rail corrugation changes. According to the formula 6 can be seen, the speed exceeds the design speed, resulting in high rail pressure increases.

5. Conclusions and Outlooks

5.1 Conclusions:

1) The vibration propagates forward in a sine wave in the discontinuous support of the distance. At the same time, according to the vibration energy at different positions, it is shown that the vibration of single point excitation exists in the track system in the form of standing waves, and the load affects the energy transfer.

2) The transmission response curves are almost identical both high and low rail under 0KN loading. When have load, the response curve will change, and the response curve will not overlap after the natural frequency, the low rail P-P frequency does not change, but the high rail P-P frequency is not obvious.

3) The rail deformation increases with the load increase, and the deformation of the lower rail is higher than that of the high rail under the same load. It coincide with the high rail energy is greater than low rail. The low rail deformation is less than the high rail, which coincide with the high rail corrugation changes.

5.2 Outlooks:

1) Analysis of the dynamic characteristics of the track system under moving source.

2) According to the hypothesis, the rail corrugation is related to the stiffness, superelevation, natural frequency, even with the difference between the high and low rail travel distance of the track system. This paper is only based on the experimental method to verify, but the quantitative relationship between the various factors has not been given, so the next step we will focus on the analysis of the quantitative relationship above those factors.

REFERENCES

1 Li Wei, Du Xing et, Investigation into the Mechanism of Type of Rail Corrugation of Metro, *journal of mechanical engineering*, **49**(16), 65–71, (2013).

2 Xu Ning, Wang Anbin. A Preliminary Study on Rail Corrugation Based on The Fractal Theory, *ICSV22*, 12-16 July, (2015).